ACS Photonics

pubs.acs.org/journal/apchd5

Letter

Nonlocal Time-Resolved Terahertz Spectroscopy in the Near Field

Angela Pizzuto,* Enrique Castro-Camus, William Wilson, Wonsik Choi, Xiuling Li, and Daniel M. Mittleman*

Cite This: *ACS Photonics* 2021, 8, 2904–2911

Read Online

ACCESS | Metrics & More | Article Recommendations

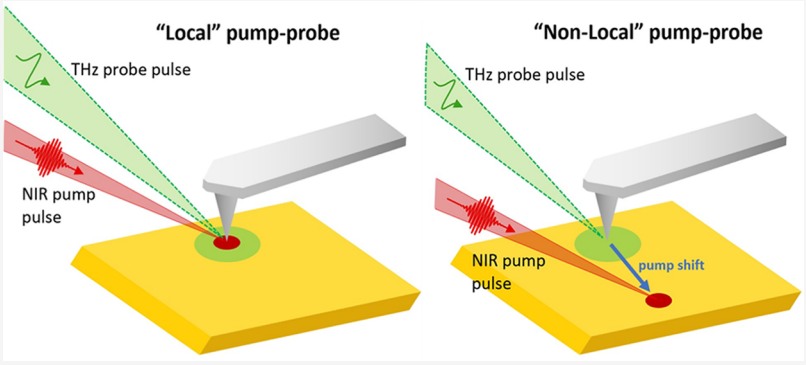

ABSTRACT: Scattering-type near-field optical microscopy (s-SNOM) has enabled subwavelength spectroscopy measurements on a wide variety of materials and over a large spectral range. These tip-based measurements are of particular interest in the long wavelength regimes, where the study of individual nanoscale samples is very challenging. The combination of s-SNOM techniques with short pulse durations has opened a new realm of possibilities in which nanosystems can be characterized with both high spatial and temporal resolution, for example via optical-pump, terahertz-probe measurements. Here, we demonstrate the first "nonlocal" pump–probe measurement using a scattering-type scanning near-field microscopy technique, in which the pump spot is laterally displaced from the probe location. We observe nonlocal effects corresponding to this pump–probe offset, associated with carrier drift into the s-SNOM near-field probe region.

KEYWORDS: *THz, s-SNOM, near-field microscopy, atomic force microscopy*

Terahertz (THz) spectroscopy is a powerful tool for characterizing charge carrier behavior in a wide variety of materials, with important applications in biosciences,[1,2] materials physics,[3−6] and chemistry.[7,8] Notably, plasma oscillations in most semiconductors occur in the terahertz regime, providing distinct spectral signatures in systems that are common in modern electronic devices.[9−11] Moreover, THz photon energies are far below these materials' bandgap, allowing for a noninvasive measurement of only the carriers that contribute to conductivity. THz time-domain spectroscopy (THz-TDS) and imaging are well-established techniques in which the electric field of the THz pulses are detected in the time domain, so all spectral information can be retrieved via Fourier transform.[12] However, conventional far-field THz-TDS is limited by diffraction and therefore cannot resolve objects much smaller than the imaging radiation wavelength. This is particularly detrimental in the long-wavelength regime, where diffraction otherwise severely limits spatial resolution and characterizing even micron-sized objects is challenging. Scattering-type scanning near-field optical microscopy (s-SNOM) has been shown to bypass this limit by several orders of magnitude;[13] a sharp, conical, conductive probe tip is held nanometers above the sample surface, spatially confining light of any wavelength near its apex and permitting imaging with a spatial resolution on the order of the tip radius, which can be far smaller than the incident wavelength. This has shown to be powerful for nanoscale characterization of bulk semiconductors,[14] nanostructures,[15,16] topological insulators,[17,18] and 2D materials[6,14,19,20] using THz radiation. Quantitative analyses of the charge carrier behavior in s-SNOM experiments are facilitated by numerous electrostatic models describing the complex interaction between the radiation, probe tip, and sample.[21−24]

In addition to these linear optical measurements, a s-SNOM approach can be employed to drastically improve the spatial

Received: September 8, 2021
Published: October 1, 2021

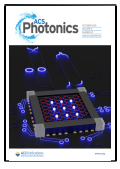

https://doi.org/10.1021/acsphotonics.1c01367
ACS Photonics 2021, 8, 2904–2911

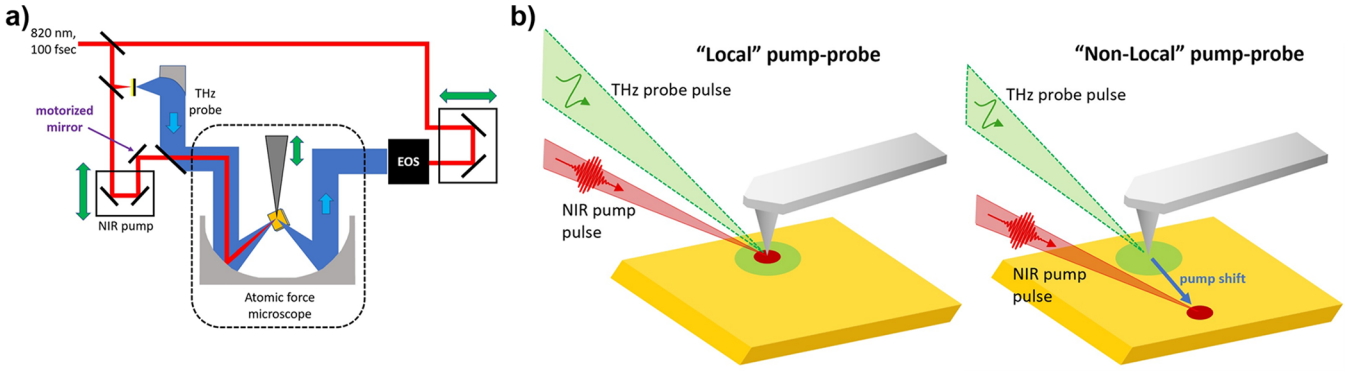

Figure 1. (a) Schematic of laser path and s-SNOM experiment. (b) Schematic of local and nonlocal pump−probe experiment, where the pump is laterally shifted relative to the probe and AFM tip to capture effects from carrier transport in materials.

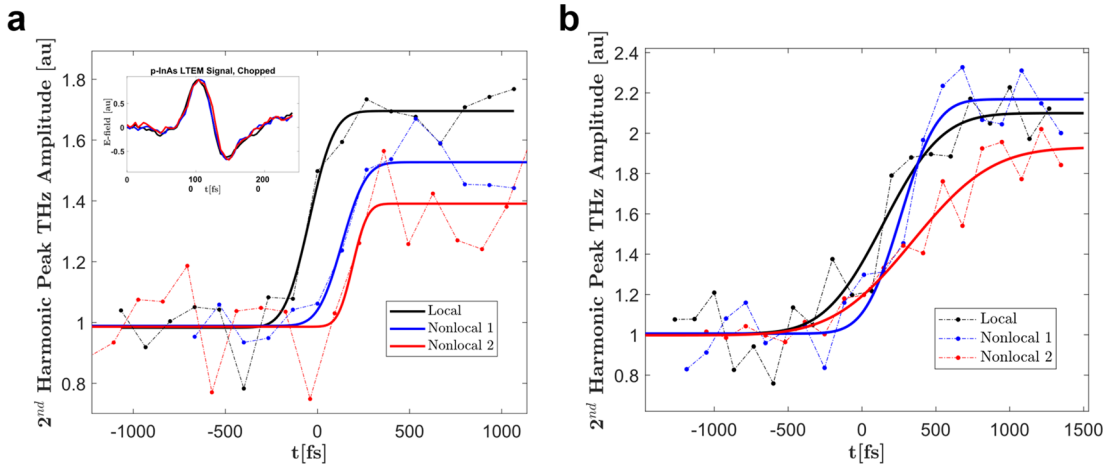

Figure 2. NIR-pump THz-probe scans showing the THz reflection as a function of time delay between pump and probe arrival. Circle markers/dashed lines show experimental data at 2nd harmonic demodulation, whereas solid lines show error function fit. (a) On bulk undoped GaAs substrate. (b) On undoped GaAs nanowire. Inset: Optically chopped p-InAs LTEM signal, showing no path length changes associated with lateral shifts in the pump spot.

resolution of nonlinear measurements such as time-resolved pump−probe experiments.[25] Numerous groups have adapted s-SNOM techniques to incorporate such capabilities,[26,27] in order to study dynamics with both high spatial and temporal resolution. Examples include studies of carrier relaxation in nanowires,[28] plasmonic behavior in exfoliated graphene,[29] and surface phonons in nanotubes.[30] In all cases, the pump and probe spot have both been localized to the tip of the scattering probe. These approaches have been effective for measuring *local* properties of the material directly underneath the metal tip. However, the use of two optical beams (i.e., pump and probe) offers an opportunity to generalize the technique to provide direct information about nonlocal effects. Numerous researchers have recognized the value of measuring nonlocal phenomena in the near field,[31−33] but the implementation of time-resolved spectroscopy remains an open challenge.

In this letter, we demonstrate the first *nonlocal* near-field pump−probe experiment. In our measurements, an ultrafast near-infrared (NIR) pulse photoexcites a sample at a location that is laterally shifted from the metallic probe tip, and the transient change in conductivity is subsequently probed with a broadband THz pulse that scatters from the metal tip. For a featureless semiconductor surface, we show that the lateral shift of the pump spot leads to a time-delayed change in the reflection of the probe radiation, consistent with carrier transport between the pump and probe spot. In a semiconductor nanowire, the direction-dependent carrier drift and diffusion leads to different behaviors depending on the direction of the lateral shift of the pump beam relative to the nanowire axis. These results, which would be impossible to observe in the far field[34] (where the diffraction-limited THz probe spot would be hundreds of microns wide, completely dwarfing the NIR pump spot), suggest many new opportunities for studying anisotropy on the nanoscale.

RESULTS AND DISCUSSION

Our s-SNOM measurements use an atomic force microscope (AFM) and PtIr-coated probe tips with ∼40 nm tip radius and 80 μm shank length to measure the reflected probe pulse via near-field THz time-domain spectroscopy (THz-TDS).[35−39] Near infrared (NIR) pulses (∼100 fs) with 820 nm center wavelength are generated by a Ti:sapphire oscillator, with 80 MHz repetition rate; these are used both as our near-field pump pulse and also for generation and detection of THz pulses. Generation is via excitation of a GaAs photoconductive antenna, which produces broadband (0.2−2 THz) terahertz pulses for use as the near-field probe. Both pump and probe spots are focused with an off-axis parabolic mirror inside the AFM, and elastically scattered off the tip−sample system. The THz radiation is detected coherently outside of the AFM using

https://doi.org/10.1021/acsphotonics.1c01367
ACS Photonics 2021, 8, 2904−2911

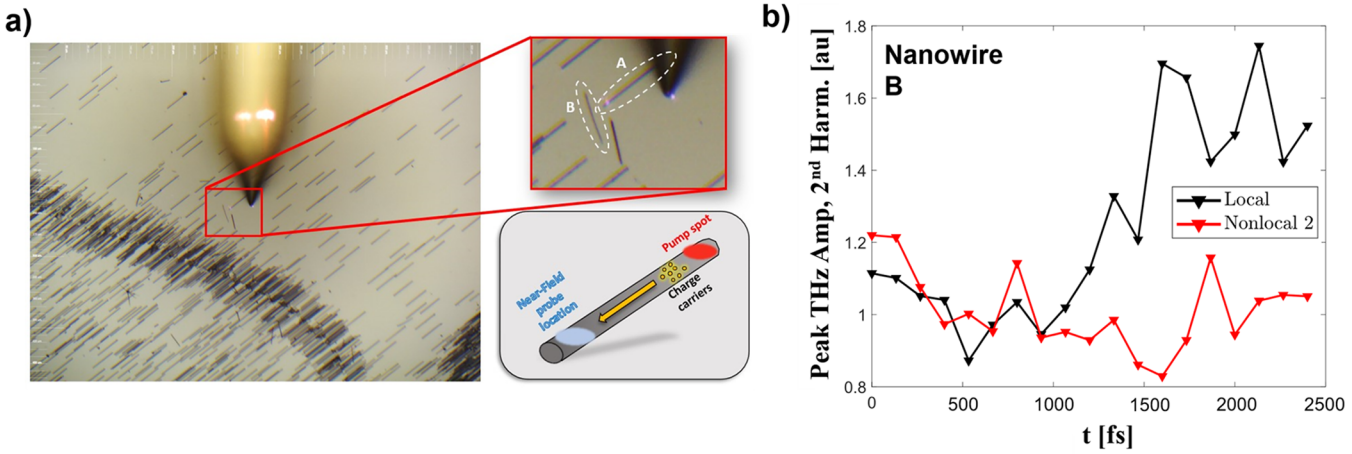

Figure 3. (a) Top-down AFM camera images of the tip and differently oriented nanowires. Top right: zoomed-in tip, pump spot, and nanowires A and B, outlined in a white dotted line. Bottom right: schematic of the nonlocal pump−probe experiment on a single nanowire, in which the pump is displaced in the nonlocal case such that we may pump one end of the nanowire and observe carrier transport via the probe on the other end. (b) Pump−probe reflectivity scans on nanowire B in the local (black) and second nonlocal position (red). We observe a strong nonlocal response, as expected, and no nonlocal response, suggesting the technique is accurately revealing the anisotropy of the nanowire structure and associated carrier transport characteristics.

free-space electro-optic (EO) sampling with a lock-in amplifier referenced to a harmonic of the tip-tapping frequency (∼26 kHz). Forward-scattered NIR radiation is blocked from the EO sampling system with a Teflon mask to ensure proper THz pulse detection. With this experimental configuration, we can either measure time-domain THz waveforms at a fixed sample position or detect the peak scattered signal (at a fixed time delay) and raster-scan the sample to generate THz near-field reflection images. For our pump−probe experiments, we measure full THz time-domain waveforms at incremental time delays between the pump and probe arrival and use the waveform peak amplitude to map the changing photoconductivity of the sample at the AFM probe tip location.[40] We measure waveforms demodulated at the second harmonic of the tip tapping frequency, and images demodulated at the third harmonic, in order to guarantee sufficient background suppression and an adequate signal-to-noise ratio.[41]

The lateral positions of the pump and probe spot are controlled independently; the NIR pump is reflected off an additional motor-controlled mirror outside of the AFM (shown in Figure 1a), which can be repositioned with 1.1 arcsecond angular resolution. We estimate, from a simple ray optics analysis, that this corresponds to a minimum lateral displacement of the illuminated spot on the sample surface of approximately 55 nm. When the NIR pump beam is centered on the location of the AFM tip, we refer to this as a "local" pump, indicating that the pump and probe beams are colocated. In contrast, a "nonlocal" measurement is one in which the pump beam is laterally shifted so that the pumped spot is different from the probed spot (see Figure 1b).

As a first step, we compare our local and nonlocal pump−probe experiments on a bare undoped GaAs wafer. Using the external positioning mirror, we first position the pump and probe together directly under the tip, as in all previous near-field pump probe measurements. We observe a rapid increase in THz reflection at zero delay with a rise time limited by the pulse durations, consistent with the expected photoconductivity response induced by our NIR pump pulse. We then laterally displace the pump spot away from this "local" positioning. With increasing lateral shift of the pump, we see an increasing time delay in the reflectivity response (see Figure 2a). As the pump spot moves further from the tip and the near-field confined probe area, a longer time is required for carriers to travel from the photoexcitation region to the tip region. We also observe a decrease in the long-time (few picosecond) limit of the reflectivity, which is consistent with a lower average photocarrier density at the probe location. We fit these THz reflection data (dotted line, circle markers) to error functions (solid lines) of the form $a\cdot\mathrm{erf}\left(\frac{t-b}{c}\right)+1$, where a is a scaling parameter, b is the inflection point, and c is a measurement of rise time. Using these fits, we extract a time delay of approximately 170 and 240 fs for the two nonlocal pump offsets shown in Figure 2a. We estimate, using our ray optics analysis, that these two nonlocal positions correspond to lateral offsets of 2.5 and 5 μm, respectively.

One possible concern is that the movement of the pump spot positioning mirror could induce a change in the arrival time of the pump pulse at the sample due to a change in the path length from the mirror to the sample. This could also lead to a shift in the pump−probe rise time, which could then be misinterpreted as due to carrier transport rather than trivial optical path length changes. To examine this possibility, we perform a time calibration by examining the arrival time of a laser terahertz emission microscopy (LTEM) signal generated by the pump pulse from a lightly p-doped InAs wafer (an excellent Photo-Dember emitter[38]), with the steering mirror in the local and two different nonlocal positions. This measurement is performed in the far-field with the same EO sampling detection system and lock-in amplifier, now referenced to an optical chopper which chops the pump beam at approximately 3 kHz. Any time delay change due to path length changes would be reflected in a change in the delay of the LTEM signal. As shown in the inset of Figure 2a, we observe that all three LTEM signals arrive at exactly the same time, regardless of mirror positioning; therefore, we conclude that any path length change due to the movement of the steering mirror is insignificant. Any time delay observed in the pump−probe rise time must therefore be due to the transport of photoexcited carriers between the pump and probe locations. It is worth

https://doi.org/10.1021/acsphotonics.1c01367
ACS Photonics 2021, 8, 2904−2911

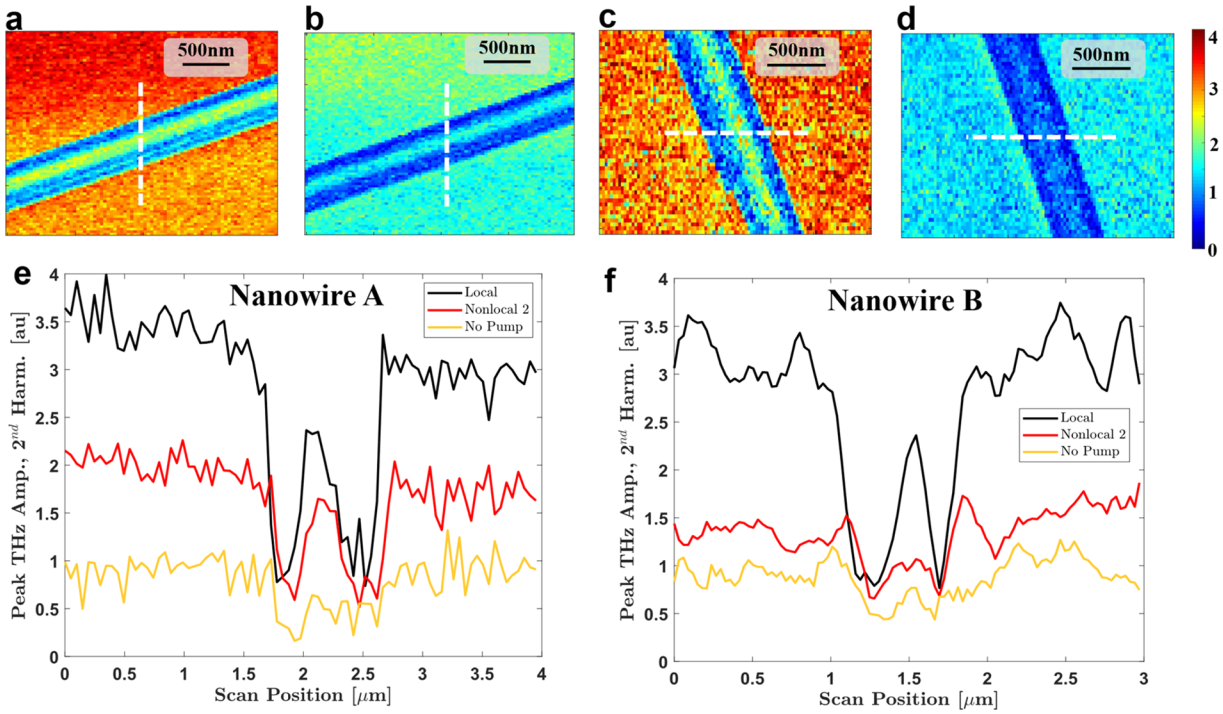

Figure 4. Normalized 2D THz probe images, 3rd harmonic demodulation. (a) Nanowire A, local position. (b) Nanowire B, local position. (c) Nanowire A, nonlocal position 2. (d) Nanowire B, nonlocal position 2. (e) Line profiles from images of Nanowire A. (f) Line profiles from images of Nanowire B. Local position shown in black, nonlocal shown in red, THz reflection with no pump shown in yellow.

noting, however, that larger mirror movement or poor alignment likely *would* induce path delay, and so this time calibration procedure must always be performed.

Next, to highlight the unique capabilities of this nonlocal pump−probe technique, we perform an identical set of measurements on a sample of undoped zincblende GaAs nanowires, lying on a GaAs substrate, grown epitaxially by metalorganic chemical vapor deposition (MOCVD) using the Au-assisted vapor−liquid−solid (VLS) method.[42−44] Because the diameters of our nanowires are quite large (~660 nm), the carrier drift/diffusion properties along the nanowire axis should be nearly identical with that of bulk GaAs;[45] however, perpendicular to this axis, carriers obviously cannot diffuse off the edge of the nanowire. We first orient the substrate such that, for a particular nanowire in a nonlocal pump positioning, one end of the nanowire is being pumped while the other is being probed (i.e., so that the lateral shift of the pump pulse is along the nanowire axis; see Figure 3a, right) As shown in Figure 2b, we observe the same behavior as in the case of the bulk GaAs substrate: for increasing lateral pump shifts, the rise time of the pump−probe signal is increasingly delayed. On the basis of the same error function fitting of the inflection point, we find good agreement among the time shifts for a given lateral shift between the nanowire and the substrate, as anticipated. Notice that the amplitude of the reflection change of the nanowire does not drop as much as it does in the bulk; this is a consequence of the confinement of the electrons, which cannot move away from the surface as they do in the bulk sample.

To confirm the directional sensitivity of the nanowire measurement, we also perform the same local and nonlocal pump−probe measurement on a nanowire which is oriented approximately 90° rotated to the one described above. This is shown in the top right panel of Figure 3a. Nanowire A is oriented along the axis of the lateral shift direction so that the pump and probe spots are both centered on the axis of the nanowire, and photocarriers can be transported along the nanowire from the pump spot to the probe spot. In contrast, nanowire B is oriented such that the nanowire is not photoexcited when the pump spot is laterally shifted, so no photocarriers should be observed at the probe spot location. The results (Figure 3b) confirm this picture; we indeed observe a strong local response in nanowire B (black curve), when the pump and probe are both focused on the AFM tip, but the nonlocal response (red curve), corresponding to the situation where the pump pulse is laterally shifted off of the edge of the nanowire, shows no pump−probe signal at all.

To further elucidate these results on differently oriented nanowires, we create THz near-field images of both wires A and B, in both the cases of local and nonlocal pumping; Figure 4 shows 2D maps of the peak probe signal for the two nanowires approximately 3 ps *after* NIR photoexcitation, when the signal has reached its plateau. We observe clear bright lines in the centers and along the axes of nanowire B in the local case (Figure 4c), and nanowire A in both cases (Figure 4a,b). This is similar to what has been seen in earlier reports of optical-pump, THz-probe studies of nanowires, corresponding to higher THz reflection and therefore higher carrier density near the central axis of the nanowire.[27] However, in the case of nonlocal pump spot positioning, nanowire B is relatively dark (Figure 4d), with no obvious carrier density increase. For a clearer comparison of the responses, Figure 4e,f show 1D cuts of these images, at positions indicated by the white dotted lines in Figure 4a−d. In both nanowires (just as in Figure 3b), a strong local response is observed, shown in Figure 4e,f as black solid lines. As anticipated, the nonlocal response remains for nanowire A (Figure 4e, red line) but disappears entirely for nanowire B (Figure 4f, red line). The very small increase in the

https://doi.org/10.1021/acsphotonics.1c01367
ACS Photonics 2021, 8, 2904−2911

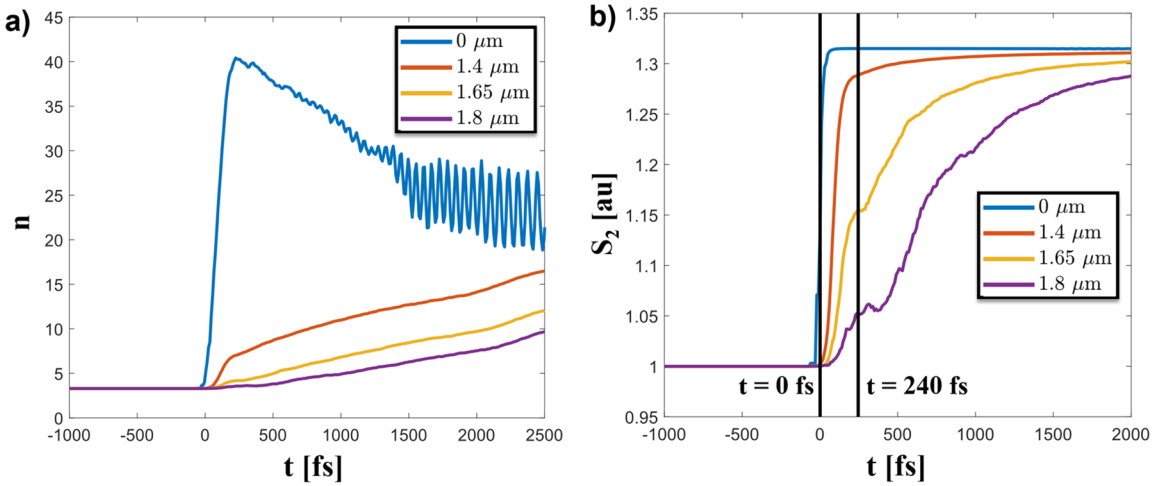

Figure 5. Numerical simulations of carrier transport in undoped GaAs. (a) Time-evolving refractive index at 0, 1.4, 1.65, and 1.8 μm away from the center of the pump spot. (b) Associated time-evolving 2nd-harmonic near-field THz probe amplitudes, calculated at 0.8 THz. 240 fs time delay observed at 1.65 μm lateral shift (yellow curves).

center of the line profile for nanowire B in this case is very similar to that observed when the pump beam is blocked (Figure 4e,f, yellow lines). We attribute this to the well-known "edge darkening" effect,[46,47] a common artifact in AFM imaging which occurs when the probe tip scans over rapidly changing topography.

In order to further corroborate the interpretation of our results, we perform a full three-dimensional semiclassical Monte Carlo simulation[48] of the carrier transport in bulk GaAs after photoexcitation by a NIR pulse. The motion of five million quasi-particles representing electrons and holes was simulated. Each particle was moved classically in 1 fs time steps, subsequently scattering probabilities were calculated for each particle, and quasi-random numbers were used to decide if each particle scatters, the scattering angle and energy loss or gain, and they recombine or become trapped. The Poisson equation is solved with the particle distribution at each time step, which is used to calculate the electric field that influences the motion of the particles in the following time-step. A very low (10^{14} cm^{-3}) intrinsic carrier population is assumed at the start of the simulation with a thermal energy distribution (300 K). Photocarriers are injected using quasi-random numbers following a temporal Gaussian distribution (FWHM = 50 fs), a Gaussian distribution across the directions parallel to the surface (FWHM = 1 μm), and an exponential distribution in the direction normal to the surface (a = 1.2 μm). The initial kinetic energy of the photocarriers follows a Gaussian distribution centered at an energy of about 0.1 eV, which is the difference between the bandgap of GaAs and the energy of the photons. Further details about the simulation can be found in prior works.[48,49] We extracted the time-dependent carrier distribution from the simulation at the surface. We then translate this into a local complex dielectric constant, accounting for both the background dielectric of the solid and that of the photocarrier plasma, using the Drude model with an expression for net total static conductivity, $\sigma^0_{\text{total}} = q(n_e\mu_e + n_h\mu_h)$, where n and μ are the local electron/hole concentrations and mobilities, respectively.[50,51]

We then employ the finite dipole model[22] (FDM), which analytically describes the tip−sample system by approximating the tip as a conductive prolate spheroid, with geometrical parameters determined from approach curve best-fits in our experiments, as described previously.[38]

Combining the FDM with the Drude model permits us to calculate the expected reflected THz signal (demodulated at second harmonic) from the tip−sample system at a frequency of 0.8 THz (the peak frequency emitted by our antenna) which we assume to be reasonably representative of the peak pulse signal. Figure 5 shows this *ab initio* prediction of the reflected THz probe signal (S_2). Figure 5a shows the predicted time-evolving refractive indices at a few selected radial distances between 0 and 2 μm from the pump pulse center. We note that the strong oscillatory behavior in the blue curve is not representative of a true physical phenomenon, but is an artifact of the simulation arising from the discrete spatial mesh. Figure 5b shows the resulting THz probe responses at these same distances. These curves qualitatively match the experimental measurements (Figure 2), showing that, the further from the center of the probe spot we pump, the weaker and more delayed is the observed change in THz reflectivity. Our simulation also reveals a strong relationship between lateral pump offset and THz signal rise time. In the local case, the GaAs is photoexcited directly underneath the tip, and the probe location detects a reflectivity increase from freed electrons and holes simultaneously. However, in the nonlocal case, the reflectivity increase corresponds to the time at which carriers diffuse underneath the tip. Because electrons are more mobile than holes in GaAs, the tip will detect mobile electrons first, then holes, and the result is a slower, more gradual rise of the pump−probe signal. This effect is visible although somewhat subtle in our experimental data, but more evident in the simulations. These simulations indicate that a nonlocal positioning that produces a 200−250 fs time delay relative to the local positioning should occur at a radial distance of approximately 1.65 μm, shown by the yellow curves. This is consistent with our estimation of the lateral shift of the probe spot in our measurements with a similar shift in delay time. Although alternative methods for calibrating the lateral pump shift at the sample location within the AFM are extremely challenging, we have separately estimated our pump shift to be on the order of a few μm using optical imaging of the sample spot combined with signal processing of these optical images. It is also worth noting that, for this prediction, the optical

https://doi.org/10.1021/acsphotonics.1c01367
ACS Photonics 2021, 8, 2904−2911

properties of the GaAs are *not* influenced by the existence of a probe tip; rather, the changing dielectric properties are a purely far-field calculation, and this behavior is *then* inserted into the FDM for near-field signal prediction. This likely accounts for the small discrepancy between the predicted (Figure 5b) and observed (Figures 2a, 2b, 3b) pump−probe response strength. Indeed, the precise interplay between the tip and optoelectronic properties can be included in the future, for more a more rigorous numerical approach. Regardless, we conclude that there is good quantitative agreement between the time delays characteristic of the simulation and those observed in our measurements, thereby confirming the utility of the nonlocal pump−probe approach for observing carrier drift and diffusion in nanomaterials.

CONCLUSION

In summary, we present the first nonlocal near-infrared pump-THz probe measurements of bulk undoped GaAs and undoped GaAs nanowires. We find a lateral shift in the pump spot relative to the probe spot yields time-shifted conductivity responses consistent with carrier mobility simulations in GaAs. We also experimentally confirm the anisotropy of undoped GaAs nanowires; a nonlocal pump positioning creates visible carrier transport only along the axis of the nanowire, whereas no conductivity change can be observed in the perpendicular orientation. This technique may be used to measure carrier drift/diffusion velocities in a variety of materials, particularly those with anisotropic optoelectronic properties.

AUTHOR INFORMATION

Corresponding Authors

Angela Pizzuto − *Department of Physics, Brown University, Providence, Rhode Island 02912, United States*; Email: angela_pizzuto@brown.edu

Daniel M. Mittleman − *School of Engineering, Brown University, Providence, Rhode Island 02912, United States*; orcid.org/0000-0003-4277-7419; Email: daniel_mittleman@brown.edu

Authors

Enrique Castro-Camus − *Department of Physics, University of Marburg, 35037 Marburg, Germany; Centro de Investigaciones en Optica A. C., Leon, Guanajuato 37150, Mexico*

William Wilson − *Center for Nanoscale Systems, Harvard University, Cambridge, Massachusetts 02138, United States*

Wonsik Choi − *Department of Electrical and Computer Engineering, Holonyak Micro and Nanotechnology Laboratory, University of Illinois at Urbana−Champaign, Champaign, Illinois 61820, United States*

Xiuling Li − *Department of Electrical and Computer Engineering, Holonyak Micro and Nanotechnology Laboratory, University of Illinois at Urbana−Champaign, Champaign, Illinois 61820, United States;* Present Address: Department of Electrical and Computer Engineering, University of Texas, Austin, Texas 78758, United States; orcid.org/0000-0003-3698-5182

Complete contact information is available at: https://pubs.acs.org/10.1021/acsphotonics.1c01367

Notes

The authors declare no competing financial interest.

ACKNOWLEDGMENTS

This work has been supported by grants from the US National Science Foundation Division of Electrical Communications and Cyber Systems, and by the Kansas City National Security Campus, operated by Honeywell Federal Manufacturing & Technologies, LLC for the United States Department of Energy under Contract No. DE-NA0002839. ECC would like to thank the support from the Alexander von Humboldt Foundation through an Experienced Research Fellowship. XL acknowledges NSF DMR 1508140 for partial support of the nanowire growth efforts.

REFERENCES

(1) Amenabar, I.; Poly, S.; Nuansing, W.; Hubrich, E. H.; Govyadinov, A. A.; Huth, F.; Krutokhvostov, R.; Zhang, L.; Knez, M.; Heberle, J.; Bittner, A. M.; Hillenbrand, R. Structural analysis and mapping of individual protein complexes by infrared nanospectroscopy. *Nat. Commun.* **2013**, *4* (1), 2890.

(2) Brehm, M.; Taubner, T.; Hillenbrand, R.; Keilmann, F. Infrared Spectroscopic Mapping of Single Nanoparticles and Viruses at Nanoscale Resolution. *Nano Lett.* **2006**, *6* (7), 1307−1310.

(3) Dai, S.; Fei, Z.; Ma, Q.; Rodin, A. S.; Wagner, M.; McLeod, A. S.; Liu, M. K.; Gannett, W.; Regan, W.; Watanabe, K.; Taniguchi, T.; Thiemens, M.; Dominguez, G.; Neto, A. H. C.; Zettl, A.; Keilmann, F.; Jarillo-Herrero, P.; Fogler, M. M.; Basov, D. N. Tunable Phonon Polaritons in Atomically Thin van der Waals Crystals of Boron Nitride. *Science* **2014**, *343* (6175), 1125−1129.

(4) Qazilbash, M. M.; Brehm, M.; Chae, B.-G.; Ho, P.-C.; Andreev, G. O.; Kim, B.-J.; Yun, S. J.; Balatsky, A. V.; Maple, M. B.; Keilmann, F.; Kim, H.-T.; Basov, D. N. Mott Transition in VO_2 Revealed by Infrared Spectroscopy and Nano-Imaging. *Science* **2007**, *318* (5857), 1750−1753.

(5) Liu, M.; Sternbach, A. J.; Basov, D. N. Nanoscale electrodynamics of strongly correlated quantum materials. *Rep. Prog. Phys.* **2017**, *80* (1), 014501.

(6) Chen, J.; Badioli, M.; Alonso-González, P.; Thongrattanasiri, S.; Huth, F.; Osmond, J.; Spasenović, M.; Centeno, A.; Pesquera, A.; Godignon, P.; Elorza, A. Z.; Camara, N.; García de Abajo, F. J.; Hillenbrand, R.; Koppens, F. H. Optical nano-imaging of gate-tunable graphene plasmons. *Nature* **2012**, *487* (7405), 77−81.

(7) Filimon, M.; Kopf, I.; Ballout, F.; Schmidt, D. A.; Bründermann, E.; Rühe, J.; Santer, S.; Havenith, M. Smart polymer surfaces: mapping chemical landscapes on the nanometre scale. *Soft Matter* **2010**, *6* (16), 3764−3768.

(8) Muller, E. A.; Pollard, B.; Raschke, M. B. Infrared Chemical Nano-Imaging: Accessing Structure, Coupling, and Dynamics on Molecular Length Scales. *J. Phys. Chem. Lett.* **2015**, *6* (7), 1275−1284.

(9) Huber, A. J.; Keilmann, F.; Wittborn, J.; Aizpurua, J.; Hillenbrand, R. Terahertz Near-Field Nanoscopy of Mobile Carriers in Single Semiconductor Nanodevices. *Nano Lett.* **2008**, *8* (11), 3766−3770.

(10) Mittleman, D. M.; Gupta, M.; Neelamani, R.; Baraniuk, R. G.; Rudd, J. V.; Koch, M. Recent advances in terahertz imaging. *Appl. Phys. B: Lasers Opt.* **1999**, *68* (6), 1085−1094.

(11) Jepsen, P. U.; Cooke, D. G.; Koch, M. Terahertz spectroscopy and imaging − Modern techniques and applications. *Laser Photonics Rev.* **2011**, *5* (1), 124−166.

(12) van Exter, M.; Fattinger, C.; Grischkowsky, D. Terahertz time-domain spectroscopy of water vapor. *Opt. Lett.* **1989**, *14* (20), 1128−1130.

(13) Mastel, S.; Lundeberg, M. B.; Alonso-González, P.; Gao, Y.; Watanabe, K.; Taniguchi, T.; Hone, J.; Koppens, F. H. L.; Nikitin, A. Y.; Hillenbrand, R. Terahertz Nanofocusing with Cantilevered Terahertz-Resonant Antenna Tips. *Nano Lett.* **2017**, *17* (11), 6526−6533.

(14) Lloyd-Hughes, J.; Jeon, T.-I. A Review of the Terahertz Conductivity of Bulk and Nano-Materials. *J. Infrared, Millimeter, Terahertz Waves* **2012**, *33* (9), 871−925.
(15) Liewald, C.; Mastel, S.; Hesler, J.; Huber, A. J.; Hillenbrand, R.; Keilmann, F. All-electronic terahertz nanoscopy. *Optica* **2018**, *5* (2), 159−163.
(16) Nguyen, T. V. A.; Hattori, A. N.; Nagai, M.; Nakamura, T.; Ashida, M.; Tanaka, H. Electrical transport properties of (La,Pr,Ca)-MnO3 nanowires investigated using terahertz time domain spectroscopy. *J. Appl. Phys.* **2016**, *119* (12), 125102.
(17) Gao, Y.; Kaushik, S.; Philip, E. J.; Li, Z.; Qin, Y.; Liu, Y. P.; Zhang, W. L.; Su, Y. L.; Chen, X.; Weng, H.; Kharzeev, D. E.; Liu, M. K.; Qi, J. Chiral terahertz wave emission from the Weyl semimetal TaAs. *Nat. Commun.* **2020**, *11* (1), 720.
(18) Park, B. C.; Kim, T.-H.; Sim, K. I.; Kang, B.; Kim, J. W.; Cho, B.; Jeong, K.-H.; Cho, M.-H.; Kim, J. H. Terahertz single conductance quantum and topological phase transitions in topological insulator Bi2Se3 ultrathin films. *Nat. Commun.* **2015**, *6* (1), 6552.
(19) Zhang, J.; Chen, X.; Mills, S.; Ciavatti, T.; Yao, Z.; Mescall, R.; Hu, H.; Semenenko, V.; Fei, Z.; Li, H.; Perebeinos, V.; Tao, H.; Dai, Q.; Du, X.; Liu, M. Terahertz Nanoimaging of Graphene. *ACS Photonics* **2018**, *5* (7), 2645−2651.
(20) Huber, M. A.; Mooshammer, F.; Plankl, M.; Viti, L.; Sandner, F.; Kastner, L. Z.; Frank, T.; Fabian, J.; Vitiello, M. S.; Cocker, T. L.; Huber, R. Femtosecond photo-switching of interface polaritons in black phosphorus heterostructures. *Nat. Nanotechnol.* **2017**, *12* (3), 207−211.
(21) Hillenbrand, R.; Keilmann, F. Complex Optical Constants on a Subwavelength Scale. *Phys. Rev. Lett.* **2000**, *85* (14), 3029−3032.
(22) Cvitkovic, A.; Ocelic, N.; Hillenbrand, R. Analytical model for quantitative prediction of material contrasts in scattering-type near-field optical microscopy. *Opt. Express* **2007**, *15* (14), 8550−8565.
(23) Govyadinov, A. A.; Amenabar, I.; Huth, F.; Carney, P. S.; Hillenbrand, R. Quantitative Measurement of Local Infrared Absorption and Dielectric Function with Tip-Enhanced Near-Field Microscopy. *J. Phys. Chem. Lett.* **2013**, *4* (9), 1526−1531.
(24) Mooshammer, F.; Huber, M. A.; Sandner, F.; Plankl, M.; Zizlsperger, M.; Huber, R. Quantifying Nanoscale Electromagnetic Fields in Near-Field Microscopy by Fourier Demodulation Analysis. *ACS Photonics* **2020**, *7* (2), 344−351.
(25) Fischer, M. C.; Wilson, J. W.; Robles, F. E.; Warren, W. S. Invited Review Article: Pump-probe microscopy. *Rev. Sci. Instrum.* **2016**, *87* (3), 031101.
(26) Nechay, B. A.; Siegner, U.; Achermann, M.; Bielefeldt, H.; Keller, U. Femtosecond pump-probe near-field optical microscopy. *Rev. Sci. Instrum.* **1999**, *70* (6), 2758−2764.
(27) Jahng, J.; Brocious, J.; Fishman, D. A.; Yampolsky, S.; Nowak, D.; Huang, F.; Apkarian, V. A.; Wickramasinghe, H. K.; Potma, E. O. Ultrafast pump-probe force microscopy with nanoscale resolution. *Appl. Phys. Lett.* **2015**, *106* (8), 083113.
(28) Eisele, M.; Cocker, T. L.; Huber, M. A.; Plankl, M.; Viti, L.; Ercolani, D.; Sorba, L.; Vitiello, M. S.; Huber, R. Ultrafast multi-terahertz nano-spectroscopy with sub-cycle temporal resolution. *Nat. Photonics* **2014**, *8* (11), 841−845.
(29) Wagner, M.; Fei, Z.; McLeod, A. S.; Rodin, A. S.; Bao, W.; Iwinski, E. G.; Zhao, Z.; Goldflam, M.; Liu, M.; Dominguez, G.; Thiemens, M.; Fogler, M. M.; Castro Neto, A. H.; Lau, C. N.; Amarie, S.; Keilmann, F.; Basov, D. N. Ultrafast and Nanoscale Plasmonic Phenomena in Exfoliated Graphene Revealed by Infrared Pump−Probe Nanoscopy. *Nano Lett.* **2014**, *14* (2), 894−900.
(30) Gilburd, L.; Xu, X. G.; Bando, Y.; Golberg, D.; Walker, G. C. Near-Field Infrared Pump−Probe Imaging of Surface Phonon Coupling in Boron Nitride Nanotubes. *J. Phys. Chem. Lett.* **2016**, *7* (2), 289−294.
(31) Li, P.; Hu, G.; Dolado, I.; Tymchenko, M.; Qiu, C.-W.; Alfaro-Mozaz, F. J.; Casanova, F.; Hueso, L. E.; Liu, S.; Edgar, J. H.; Vélez, S.; Alu, A.; Hillenbrand, R. Collective near-field coupling and nonlocal phenomena in infrared-phononic metasurfaces for nano-light canalization. *Nat. Commun.* **2020**, *11* (1), 3663.
(32) Kaneta, A.; Hashimoto, T.; Nishimura, K.; Funato, M.; Kawakami, Y. Visualization of the Local Carrier Dynamics in an InGaN Quantum Well Using Dual-Probe Scanning Near-Field Optical Microscopy. *Appl. Phys. Express* **2010**, *3* (10), 102102.
(33) Kaneta, A.; Fujimoto, R.; Hashimoto, T.; Nishimura, K.; Funato, M.; Kawakami, Y. Instrumentation for dual-probe scanning near-field optical microscopy. *Rev. Sci. Instrum.* **2012**, *83* (8), 083709.
(34) Yao, Z.; Chen, X.; Wehmeier, L.; Xu, S.; Shao, Y.; Zeng, Z.; Liu, F.; McLeod, A. S.; Gilbert Corder, S. N.; Tsuneto, M.; Shi, W.; Wang, Z.; Zheng, W.; Bechtel, H. A.; Carr, G. L.; Martin, M. C.; Zettl, A.; Basov, D. N.; Chen, X.; Eng, L. M.; Kehr, S. C.; Liu, M. Probing subwavelength in-plane anisotropy with antenna-assisted infrared nano-spectroscopy. *Nat. Commun.* **2021**, *12* (1), 2649.
(35) von Ribbeck, H. G.; Brehm, M.; van der Weide, D. W.; Winnerl, S.; Drachenko, O.; Helm, M.; Keilmann, F. Spectroscopic THz near-field microscope. *Opt. Express* **2008**, *16* (5), 3430−3438.
(36) Aghamiri, N. A.; Huth, F.; Huber, A. J.; Fali, A.; Hillenbrand, R.; Abate, Y. Hyperspectral time-domain terahertz nano-imaging. *Opt. Express* **2019**, *27* (17), 24231−24242.
(37) Moon, K.; Park, H.; Kim, J.; Do, Y.; Lee, S.; Lee, G.; Kang, H.; Han, H. Subsurface nanoimaging by broadband terahertz pulse near-field microscopy. *Nano Lett.* **2015**, *15* (1), 549−52.
(38) Pizzuto, A.; Mittleman, D. M.; Klarskov, P. Laser THz emission nanoscopy and THz nanoscopy. *Opt. Express* **2020**, *28* (13), 18778−18789.
(39) Klarskov, P.; Kim, H.; Colvin, V. L.; Mittleman, D. M. Nanoscale Laser Terahertz Emission Microscopy. *ACS Photonics* **2017**, *4* (11), 2676−2680.
(40) Beard, M. C.; Turner, G. M.; Schmuttenmaer, C. A. Transient photoconductivity in GaAs as measured by time-resolved terahertz spectroscopy. *Phys. Rev. B: Condens. Matter Mater. Phys.* **2000**, *62* (23), 15764−15777.
(41) Wang, L.; Xu, X. G. Scattering-type scanning near-field optical microscopy with reconstruction of vertical interaction. *Nat. Commun.* **2015**, *6*, 8973−8973.
(42) Fortuna, S. A.; Wen, J.; Chun, I. S.; Li, X. Planar GaAs Nanowires on GaAs (100) Substrates: Self-Aligned, Nearly Twin-Defect Free, and Transfer-Printable. *Nano Lett.* **2008**, *8* (12), 4421−4427.
(43) Choi, W.; Seabron, E.; Mohseni, P. K.; Kim, J. D.; Gokus, T.; Cernescu, A.; Pochet, P.; Johnson, H. T.; Wilson, W. L.; Li, X. Direct Electrical Probing of Periodic Modulation of Zinc-Dopant Distributions in Planar Gallium Arsenide Nanowires. *ACS Nano* **2017**, *11* (2), 1530−1539.
(44) Miao, X.; Chabak, K.; Zhang, C.; Katal Mohseni, P.; Walker, D.; Li, X. High-Speed Planar GaAs Nanowire Arrays with f max > 75 GHz by Wafer-Scale Bottom-up Growth. *Nano Lett.* **2015**, *15*, 2780.
(45) Joyce, H. J.; Docherty, C. J.; Gao, Q.; Tan, H. H.; Jagadish, C.; Lloyd-Hughes, J.; Herz, L. M.; Johnston, M. B. Electronic properties of GaAs, InAs and InP nanowires studied by terahertz spectroscopy. *Nanotechnology* **2013**, *24* (21), 214006.
(46) Bek, A.; Vogelgesang, R.; Kern, K. Apertureless scanning near field optical microscope with sub-10nm resolution. *Rev. Sci. Instrum.* **2006**, *77* (4), 043703.
(47) Taubner, T.; Hillenbrand, R.; Keilmann, F. Performance of visible and mid-infrared scattering-type near-field optical microscopes. *J. Microsc.* **2003**, *210* (3), 311−314.
(48) Johnston, M. B.; Whittaker, D. M.; Corchia, A.; Davies, A. G.; Linfield, E. H. Simulation of terahertz generation at semiconductor surfaces. *Phys. Rev. B: Condens. Matter Mater. Phys.* **2002**, *65* (16), 165301.
(49) Castro-Camus, E.; Lloyd-Hughes, J.; Johnston, M. B. Three-dimensional carrier-dynamics simulation of terahertz emission from photoconductive switches. *Phys. Rev. B: Condens. Matter Mater. Phys.* **2005**, *71* (19), 195301.
(50) Arora, N. D.; Hauser, J. R.; Roulston, D. J. Electron and hole mobilities in silicon as a function of concentration and temperature. *IEEE Trans. Electron Devices* **1982**, *29* (2), 292−295.

https://doi.org/10.1021/acsphotonics.1c01367
ACS Photonics 2021, 8, 2904−2911

(51) Ashcroft, N. W.; Mermin, N. D. *Solid State Physics*; Saunders College Publishing, 1976.

https://doi.org/10.1021/acsphotonics.1c01367
ACS Photonics 2021, 8, 2904−2911